UKAEA RESEARCH GROUP

Preprint

OBSERVATIONS OF LARGE AMPLITUDE HELICAL KINK INSTABILITIES AND FIELD REVERSAL IN A FAST PINCH EXPERIMENT (HBTX-I)

A J L VERHAGE
A S FURZER
D C ROBINSON

CULHAM LABORATORY
Abingdon Oxfordshire

1976

OBSERVATIONS OF LARGE AMPLITUDE HELICAL KINK INSTABILITIES AND FIELD REVERSAL IN A FAST PINCH EXPERIMENT (HBTX-1)

A J L Verhage, A S Furzer, D C Robinson
Culham Laboratory, Abingdon, Oxon, OX14 3DB,UK
(Euratom/UKAEA Fusion Association)

ABSTRACT

Amplification of toroidal flux in compressed stabilized z-pinches in HBTX-1 (R = 100 cm, a = 6 cm) has been observed during MHD instabilities. The increase in flux leading to reversal of longitudinal magnetic field in the outside region when the toroidal flux is conserved is attributed to the large amplitude stage of an m=1 helical kink instability, which redistributes the magnetic field. The measured values of wavelength, amplitude, and growth rate in the early stages of the m=1 instability observed during self reversal are predicted with linear MHD stability computations which include dissipative effects. The observed radial expansion of the plasma is interpreted as a non-linear effect associated with the large amplitude stage of the instability. After the process of self reversal an approximately constant value of the pinch ratio is obtained, which is independent of the initial parameters of the pinch.

August 1976

CONTENTS   Page

1. INTRODUCTION

In many experiments with stabilized pinches in linear and toroidal geometry the longitudinal magnetic flux inside the plasma vessel is observed to increase during the induction of plasma current. Part of this increase in flux can be explained by the pinch effect and anisotropy of electrical conductivity (the paramagnetic effect[1]), but additional effects are necessary to account for the observations. When the longitudinal flux is conserved enhancement of the longitudinal flux inside the plasma is accompanied by a reduction and often reversal of the longitudinal field outside. Theoretically in a flux conserving system the longitudinal magnetic field averaged over an annular region outside the plasma cannot change sign by motions in two dimensions alone[2-4], so plasma motions in the azimuthal plane associated with field reversal must be accompanied by motions in the longitudinal direction.

Naturally occurring field reversal was observed in the late 1950's in many toroidal pinch devices; for example in the Mark IV-torus[5], Zeta[6], Alpha[7], Gamma[8], Perhapsatron[9] and Sceptre[10].

Kadomtsev[11] studied the phenomenon theoretically in 1961 and proposed local convective instabilities leading to force free configurations as a possible mechanism for the generation of field reversal. Helical equilibria of pinches with negligible pressure gradients were also described by Kadomtsev and applied to explain experimental results in the linear Columbus experiment[12]. At that time Kadomtsev rejected the model in which the plasma column changes from cylindrical to solenoidal due to an m=1 helical kink mode because the product of wavenumber k and amplitude r_o of helical kink instabilities measured in slow pinch experiments was too small to explain the increase in magnetic flux[5] (for example: too small by a factor of 5 in Zeta).

In recent experiments with smaller dimensions on Eta-Beta[13], FRSX[14] and HBTX[15-18], in which the rise time of the plasma current is comparable with the growth time of instabilities, field reversal is found which is associated with m=1 helical kink instabilities. In this paper naturally occurring field reversal observed under such conditions in toroidal pinch experiments on HBTX-1 is described. The properties of the m=1 helical kink instabilities such as wavelength, growth rate, and field perturbations measured during the exponential growth of the instabilities are found to agree well with theoretical predictions from linear MHD codes, which include dissipative effects. The occurrence of reversed field is observed to be associated with the large amplitude stage of the instability. The final effect of the non-linear stage of the instability is a radial expansion of the plasma followed by an approximately axisymmetric reversed field state.

The pinch ratio $\Theta(r_1)$, defined as the ratio of the average value of B_θ at the wall to B_z averaged over the plasma, falls as a result of the flux increase during the instability until a final value of about 1.6 is reached. This final value is observed to be independent of the initial value of $\Theta(r_1)$, as shown in figure 1 where reversal of magnetic field occurs during large amplitude m=1 helical instabilities. The evolution towards a state with constant pinch ratio, as observed in HBTX-1, was reported in Lausanne[17], where it was interpreted with the help of Taylor's theory[19] as a relaxation towards a state with minimum magnetic energy. The mechanism of relaxation is not explained by this theory.

The non-linear stage of the instability is discussed and simple models are presented which can explain field reversal and plasma expansion. In particular it is shown that for HBTX-1 the solenoidal effect of the helix characterized by kr_o is sufficiently large to account for the observed flux enhancement and field reversal.

2. DESCRIPTION OF THE MEASUREMENTS IN HBTX-1

2.1 The experimental device

The dimensions of the torus of the High Beta Toroidal Experiment (HBTX) are as follows: major radius R = 100 cm, inner radius of the quartz wall r_1 = 6 cm, inner radius of the metal shell r_2 = 7.5 cm, effective radius of the toroidal flux boundary in a crowbarred experiment r_3 = 9.8 cm. The radius of the plasma r_p is defined as the radius for which the plasma pressure decreases to half the maximum value. A stabilized z-pinch is produced by crowbarring the toroidal field coils with metal-to-metal switches when a predetermined value of the toroidal field is reached, followed by the induction of plasma current. The deuterium gas at a filling pressure of 40 mtorr, is not pre-ionized. The compression rate r_1/r_p is controlled by the ratio of plasma current to trapped longitudinal flux, usually represented by the pinch ratio Θ, taken at the boundary r = r_1, where $\Theta(r_1) = \mu_o r_1 I / 2\Phi(r_1)$. The metal shell of the torus is split along a major diameter and the two halves are connected in parallel to a capacitor bank with C = 336 µF and V_o = 34 kV. The induced plasma current rises to 150 kA in 16 µs for an initial toroidal field of 3.3×10^{-2} T and is then crowbarred with metal-to-metal switches.

2.2 Diagnostics

The evolution of a compressed stabilized z-pinch in HBTX-1 is studied with magnetic pick-up coils and streak photography. The radial distribution of magnetic field inside the plasma is measured with an array of 11 coils, mounted 4 mm apart on a former with a diameter of 2 mm, which can be rotated to pick-up either the z- or the θ-component of the magnetic field. A twelfth coil measures the radial magnetic field. The former with the 12 coils is positioned vertically inside a quartz envelope, outer diameter 3.5 mm. The influence of the probe on the plasma was checked by varying the position of the envelope for fixed positions of the coil. The insertion of the

envelope into the plasma is observed to cause an earlier onset of the instability by $\tilde{\sim}$ 0.5 µs. The effect of the probe does not alter the parameters of the instability as measured outside the plasma, near the position of the probe.

The azimuthal dependence of the 3 components of the magnetic field is measured at 8 positions near the metal wall. Integral coils are used to determine the average of B_z and B_θ over minor azimuth, and their average weighted by $\sin \theta$ and $\cos \theta$ (sine and cosine-coils).

The toroidal flux is determined with loops around the plasma vessel. The current in toroidal field coils, the total toroidal current in the plasma, and the current in the primary circuit are measured with Rogowski-coils. Time correlation to 200 ns is achieved using analog-digital converters.

3. MEASUREMENTS OF INSTABILITY AND FIELD REVERSAL IN A STABILIZED Z-PINCH

Experimental data is presented for a stabilized z-pinch with an initial value of the stabilizing field $B_z(t=0) = 3.3 \times 10^{-2}$ T. The plasma becomes unstable to a gross m=1 helical kink mode when the plasma current rises above 70 kA and the compression ratio exceeds 2.5 The onset time of m=1 instabilities varies with the value of $B_z(t=0)$. Amplification of the toroidal flux inside the plasma is always observed during the initial compression of the plasma. The extra increase in flux which occurs later in time together with field reversal is associated with the m=1 helical kink instability, in conditions studied so far.

3.1   The growth of the m=1 helical instability

The main parameters of the evolving stabilized z-pinch, measured with electrical diagnostics outside the plasma are shown in figure 2. The initial compression is characterized by an increase in toroidal flux inside the plasma as shown by the traces of $\Phi(r_2)$ and $d\Phi(r_2)/dt$ in figure 2. This increase is concurrent with a fall in B_z outside the plasma, while the total toroidal flux $\Phi(r_3)$ is conserved. The crowbarred primary current in the toroidal field coils is a measure of the field outside the plasma averaged over a quarter section of the torus. This signal is marked $<B_z(r_2)>$ whereas $B_z(r_2)$ is the local azimuthal average measured with annular coils. The voltage across one of the gaps in the shell is proportional to the applied toroidal electric field.

By the time the plasma is compressed to a radius r_p = 2 cm (deduced from the pressure profile in figure 12) at t = 4.5 µs after the start of the plasma current, the dI/dt signal shown in figure 2 is observed to decrease over a period of 1 µs; this corresponds to an increase in inductance. While dI/dt approaches a minimum value an amplification of $\Phi(r_2)$ is observed at t = 5.2 µs and $<B_z(r_2)>$ reverses. The fall in $\Phi(r_1)$ in figure 1, waveform 2, is a result of the increase in $\Phi(r_1) = \Phi(r_2) - \pi(r_2^2 - r_1^2) <B_z(r_2)>$.

In figure 3 the enhancement of the toroidal flux is seen to occur simultaneously with the rise in amplitude of the signals from sine and cosine coils. At the same time a discontinuity in the $B_z(r_2)$ waveform is observed, which is not seen in the averaged value $<B_z(r_2)>$ shown in figure 2.

The displacement of the electron density distribution is derived from the streak photograph in figure 4, which shows the light intensity in the continuum, $\lambda = 535 \pm 15$ nm. The onset time and amplitude of the displacement inferred from sine and cosine coils, assuming a straight displaced plasma current channel, agree well with the optically deduced onset time and displacement amplitude during the growth of the instability, as shown in figure 5. The displacement amplitude Δ of a straight current filament inside a conducting cylinder is expressed as the ratio of the first and zeroth harmonic of B_θ, measured at the conducting wall: $\Delta = r_2 B_{\theta 1}(r_2)/2 B_{\theta 0}(r_2)$ [20-22]. The output of a sine-coil and a cosine-coil is proportional to $B_{\theta s}$ and $B_{\theta c}$ where $B_{\theta s} = \frac{1}{\pi} \int_0^{2\pi} B_\theta(r_2, \theta) \sin \theta \, d\theta$ and $B_{\theta c} = \frac{1}{\pi} \int_0^{2\pi} B_\theta(r_2, \theta) \cos \theta \, d\theta$, and $B_{\theta 1} = \left(B_{\theta s}^2 + B_{\theta c}^2 \right)^{\frac{1}{2}}$. If the current channel is assumed to be helical instead of straight the displacement must be corrected for the wavenumber and the radius of the helix [20,21]. The magnitude of the displacement of the plasma column derived from a given signal increases from 2.5 cm for a straight plasma colum to 3.5 cm for a helical plasma with a wavelength of 20 cm, parameters typical for t>5.5 μs in figure 5. The displacement seen in figure 5 before the instability occurs is due to an outward shift of the plasma column of on average 6 mm, which is interpreted as the toroidal equilibrium shift. The position of the current centre in the r-θ plane is derived from the phase difference between the signals from the sine and cosine coils. The amplitude of the locus of $B_{\theta 1}/B_{\theta 0}$ in figure 6 is proportional to the displacement of a straight current channel. The centre of the current distribution is deduced to rotate away from the horizontal plane during the m=1 instability. A similar rotation of the plasma column is observed optically from stereoscopic views of the plasma monitored with a streak camera, as illustrated in figure 13.

The normal mode numbers m and k of the field perturbations measured during the growth of the instability are determined with electrical diagnostics (section 2.2). The wavenumber k follows from the angle of the perturbed field at the wall, generally expressed as $kr = m\, B_{zm}(r,\theta)/B_{\theta m}(r,\theta)$, with $B = B_O + \sum_{m=1}^{\infty} B_m \cos(m\theta + kz)$. For m=0 the wavelength at the wall is $k = \frac{1}{B_{zo}} \frac{\partial B_r}{\partial r}$. Azimuthal mode numbers are obtained by Fourier analysis of the perturbations of the magnetic field near the metal wall, measured at 8 positions round the tube. The assignment of mode number to instabilitities inside the plasma by Fourier analysing the field outside the plasma can be done for gross modes by which the whole plasma column is distorted, but is more difficult for highly localized modes inside the plasma.

The early stages of the instability $5.2 < t < 5.6$ μs are characterized by m=1 and a decreasing value of k, which is on average about 60 m^{-1} (corresponding to a wavelength of 10 cm). The time dependence of k for one discharge is shown in figure 7 where $kr = B_{z1}/B_{\theta 1}$ is measured near the conducting wall at r = 7 cm. The sign of $B_{z1}/B_{\theta 1}$ is opposite to the sign of $B_{z0}/B_{\theta 0}$ before field reversal. During the growth of the instability $\langle B_z(r_2)\rangle$, shown in figure 2, reverses .

Magnetic field perturbations $\delta B_\theta, \delta B_z$ inside the plasma are obtained as the difference between the extrapolated unperturbed field and the actual field, both shown in figure 8 during the growth of the instability. The field perturbations, plotted in figure 9, are observed to grow from r $\approx$ 2 cm with an exponential growth time of 0.4 μs, a value similar to the growth time for the displacement in figure 5. The pitch length of the mean field, defined as $2\pi r\, B_z/B_\theta$, is about 10 cm in this region, increasing in time since the perturbations cause B_z to rise while B_θ falls. It is seen that the sign of $\delta B_z/\delta B_\theta$ is opposite to the sign of the pitch of the unperturbed field. Perturbations are also measured near the axis and in the outside region

at $r \sim 5$ cm where B_z is reversed while B_θ is reduced. Comparison between
the distributions at $t = 5.0$ µs and $t = 5.6$ µs indicates that the longitudinal
flux has grown at the expense of the azimuthal flux, even when corrections
for the non-axisymmetry at $t = 5.6$ µs are made.

3.2 The large amplitude stage of the instability

The instability associated with field reversal has reached the large
amplitude stage when the perturbations are no longer small compared with the
mean field and the displacement amplitude is of the same order of magnitude
as the radius of the wall. In the non-linear stage instabilities can no
longer be represented by a single pair of mode numbers (m,k).

The main features of the large amplitude stage are also seen in figure 2.
The value of dI/dt falls until $t = 6$ µs when dI/dt rapidly increases on a
timescale for which changes in the external circuit can be ignored, thus
indicating a drop in plasma inductance, i.e. an expansion of the current carrying
column. Meanwhile $d\Phi(r_2)/dt$ continues to rise and reaches maximum at the same
time as dI/dt. The fall in inductance is also reflected by the gap voltage which
shows a negative step. The averaged field outside the plasma $<B_z(r_2)>$ is directly
related to $\Phi(r_2)$ as expected from the conservation of $\Phi(r_3)$, but $B_z(r_2)$ exhibits
a spike before the average level of reversal is attained. After the instability
has saturated the further increase in flux becomes relatively small. From the streak
photographs in figures 4 and 13 it is concluded that the plasma reaches the
wall in the large amplitude stage. The wavelength associated with the first
azimuthal harmonic of the large amplitude field perturbations has then increased
to 40 cm or $k = 15$ m^{-1}, while the direction of the displacement, represented
by $B_{\theta 1}/B_{\theta 0}$ in figure 7, continues to move in the r-θ plane. The spectrum of
azimuthal modes is given in figure 10 by the B_z-perturbations measured at
the wall as a function of time. The perturbation amplitude appears in figure 10
as the radial distance from the circle for which $\delta B_z(r_2,\theta) = 0$. After the

initial m=1 shift an averaged value of reversed field of $6-8 \times 10^{-2}$T.is observed, but the magnitude of $B_z(r_2)$ varies as a function of θ. Superimposed on the reversed field are harmonics with $m \geqslant 1$ and at some points the field is not reversed at all.

The magnetic fields, of which profiles are shown in figure 8 and figure 12, are redistributed during the instability, which results in a radial expansion of the field configuration. The B_z-perturbations, shown in figure 9, are expected to cause a flux amplification inside the plasma which is indeed observed with flux loops. The field reversal is then a necessary consequence of the conservation of total toroidal flux.

The relation between longitudinal (toroidal) flux Φ and azimuthal (poloidal) flux χ has been studied by crowbarring the primary toroidal current circuit just before the instability (t = 5 µs). In figure 11 the total increase in $\Phi(r_1)$ is shown to be equal to the reduction in $\chi(r_1)$, when averaged over the full period of instability (5<t<7 µs) provided the effective wavelength is 10 cm, so that the helical flux $\psi(r_1) = \Phi(r_1) + \chi(r_1)$ is conserved. The graph of figure 11 was constructed from data of 8 discharges which reduces the effect of random motions. The values of $\Phi(r_1)$ from probe data in figure 11 agree within 20% with the values from flux loops. The averaged wavelength of 10 cm or $k = 60$ m^{-1} derived from the change in flux between t = 5 µs and t = 7 µs is only observed at the wall during the early stages of the m=1 instability when perturbations are small compared with the mean field (linear stage).

3.3 The development of the reversed field pinch

The non-linear stage of the instability is followed by a reduction in the amplitude of the m=1 mode and an approximate restoration to axisymmetry. A recurrence of the m=1 instability is observed for t > 8 μs while the plasma current continues to rise with a risetime of 16 μs. The m=1 displacement measured by $B_{\theta 1}/B_{\theta 0}$ in figure 6 is seen to reach a minimum between t = 7 μs and t = 8 μs. The perturbation amplitude of B_z, shown in figure 10 as a function of azimuthal angle has become axisymmetric at t = 7.5 μs. The occurrence of an m=1 instability followed by a period of axisymmetry is observed several times during the discharge, but the first instability at t > 5 μs has the largest effect on the field distribution as shown by the measured field profiles in figure 12. The contraction of the field profiles, observed before the occurrence of an instability, is countered by enhancement of B_z and reduction of B_θ during an instability. The longitudinal flux increases as long as the plasma current rises but much more slowly than during the first instability, while the pinch ratio $\Theta(r_1)$ stays constant.

The $B_\theta = 0$ line deviates from the geometrical centre for most of the time (for t > 5 μs), so the magnetic axis is shifted with respect to the geometrical axis. The luminosity profile on the streak photographs in figures 4 and 13 is observed to reach the wall at t ≈ 6 μs after which the light emission appears to originate mainly from the wall and from filamentary structures inside the tube. When the primary circuit is crowbarred at t = 16 μs the field configuration decays while gross m=1 instabilities continue to occur. The average value of B_z outside the plasma stays reversed until t = 40 μs. The plasma current and toroidal flux decay with the same decay time while $\Theta(r_1)$ remains approximately constant.

4. DISCUSSION OF THE EXPERIMENTAL RESULTS AND COMPARISON WITH THEORY

4.1 Comparison with linear MHD-stability theory

The early stage of the helical kink instability is characterized by mode numbers m=1 and k changing from 100 m^{-1} to 30 m^{-1}, as determined outside the plasma. The instability is shown to originate near r = 2 cm where the pitch of the perturbations and the pitch of the unperturbed field have opposite sign. The increase in the inductance for the plasma current, observed during the growth of the helical kink, is understood as the transition of the current channel from axisymmetric to helical. The nature of such an instability has been investigated with linear MHD stability codes.

The magnetic field distributions of figure 12 measured before field reversal is observed, were tested for stability against MHD-modes with numerical codes. These are 1D MHD computer programmes with $\sigma=\infty$, σ=finite and σ,χ,ν=finite, where σ,χ,ν are electrical conductivity, thermal conductivity and viscosity respectively.

Results from the ideal MHD code[23] and resistive MHD codes[24-26] have been published before. The three programmes permit the computation of growth rates, displacement amplitudes and field perturbations as a function of radius, for preselected mode numbers m and k, for a given magnetic pitch $P(r) = rB_z/B_\theta$. The resistive codes require a smooth analytic function to match the measured pitch as input data. Introduction of the pitch leaves the freedom to vary β_θ in order to check the effect of pressure on the stability ($\beta_\theta \equiv 8\pi Nk(\overline{T}_e + \overline{T}_i)/\mu_o I^2$), where N is the line density, $k\overline{T}_e$ and $k\overline{T}_i$ are the averaged energy of electrons and ions respectively. The value of β_θ derived from the magnetic field profile at t = 5 μs, assuming magnetostatic equilibrium, is 0.6.

Results from the ideal MHD code with β_θ = 0.6 and allowing for plasma compression are shown in figure 14, where the growth rate is plotted as a function of wavenumber, (kP < 0).

For wavelengths longer than about 5 cm m=1 is predicted to be the dominant mode with shortest growth times at t = 5 µs of about 0.6 µs; m=2 is stable and m=0 grows more slowly by a factor 2-3, but for $\lambda < 5$ cm growth times of m=1 and m=2 are shorter than 1 µs. Growth rates computed with the same ideal MHD-code for the pitch derived directly from the measured fields, and for the matched analytic pitch function are shown in figure 14 and figure 15 respectively. The difference in growth rates for $\lambda < 5$ cm is a result of the sensitivity of shorter wavelength modes to the precise radial dependence of the pitch. These modes are pressure driven modes due to the violation of Suydam's local criterion.

The introduction of dissipative effects smoothes the local gradients and reduces the growth rates of m=1 and m=2 by about an order of magnitude for $\lambda < 5$ cm as seen in figure 15. The dominant mode is therefore predicted to be m=1 with $30 \leq k \leq 60$ m^{-1} at maximum growth rate, which corresponds to growth times between 0.9 µs and 1.2 µs depending on the dissipation. The growth time for m=0 is still 2-3 times longer than the growth for m=1, so the m=0 mode is not likely to be observed.

The wavenumber for m=1 is well within the range of experimental values observed during the early stages of the instability. The measured growth time is about 0.4 µs at t = 5.5 µs but the plasma current is then 30% higher than at t = 4 µs. The computed growth rates of figure 15 must therefore be increased by 30% to be compared with the experimental values, thus the predicted minimum growth time for the case with finite σ is reduced to 0.6 µs while for finite σ,χ,ν 0.85 µs is found. The nature of the m=1 mode is investigated by reducing β_θ for the given pitch function. The computed growth rate for m=1, $|k| < 100$ m^{-1} hardly depends on β_θ, hence the driving energy comes from the azimuthal magnetic field rather than from the pressure gradient. The position of the conducting wall has been varied in the computations to check the influence of wall stabilization. For $|k| < 100$ m^{-1} the growth rates with and without dissipation do not change when the conducting wall is moved outwards, so the plasma is already too compressed for wall

- 12 -

stabilization to play a role for both ideal MHD modes and dissipative modes.

The Lundquist number used in computations for figure 15 is
$S = 100$, though similar results are also obtained at $S = 1000$. In the
experiment $100 < S < 1000$. (S is the ratio of diffusion time to hydromagnetic
transit time across the radius of the tube).

The influence of resistivity on field perturbations computed for the field
profiles at $t = 4$ μs for $m=1$, $k = 60$ m^{-1} ($\lambda = 10$ cm) is illustrated in figure 16,
where again it is shown that the instability is adequately described by ideal
MHD theory, and is insensitive to the precise configuration. The differences
in the field perturbations due to the matching of the measured radial dependence
of the pitch by an analytic function are also shown in figure 16. The
magnetic field perturbations computed for the field distributions at $t = 5$ μs
are compared with the perturbations measured during the growth of the instability
at $t = 5.4$ μs and $t = 5.8$ μs in figure 17. The perturbed field distributions
for $r < 4$ cm measured at $t = 5.4$ μs are shown to match the profiles computed
for an $m=1$ mode with $k = 60$ m^{-1}. The computed profiles for $m=0$, $k = 60$ m^{-1}
have a smaller amplitude by about a factor of 3 and do not agree with the
measured profiles.

The δB_θ profiles for $r < 4$ cm measured at $t = 5.8$ μs are still in good
agreement with the computed δB_θ distribution for $m=1$, $k = 60$ m^{-1} in spite of
the large amplitude of the perturbation ($\delta B_\theta/|B| \approx 0.3$). The negative value of
δB_z in the centre and the δB_z amplitude for $r > 5$ cm, which reverses the field
in the outside region, are not predicted with the linear MHD code. The
perturbations in the outside region indicate that plasma current flows near
the wall, which is interpreted as a non-linear effect of the instability. The
flux associated with δB_z inside the plasma is not conserved for the measured
distribution at $t = 5.8$ μs, contrary to the predictions with linear MHD theory
on which the numerical computations are based. The linear MHD mode with $m=1$,
$k = 60$ m^{-1} and growth rate of 0.6 μs is predicted to produce field perturbations

which explain the experimentally observed perturbations until non-linear effects become important. The measured growth time of 0.4 μs is shorter than the predicted value but approximations in the theory and measuring errors can account for the discrepancy.

4.2 Discussion of the large amplitude stage of the instability

A number of observed phenomena are interpreted as a consequence of the non-linear behaviour of the m=1 helical kink instability, including the amplification of toroidal flux inside the plasma and hence the reversal of the field outside the plasma; the large changes in inductance of the plasma current – an increase in inductance during the growth of the instability followed by a fall in inductance when the amplitude of the instability is maximal; also the redistribution of magnetic field, the approximate restoration of axisymmetry when the instability has saturated, and the difference between $B_z(r_2)$ and the average value $<B_z(r_2)>$. A model describing the plasma as a filament seems a reasonable first approximation to gain some understanding of the large amplitude stage of the helical m=1 instability, since the plasma radius r_p at the onset of instability is 2 cm, small compared with the radius of the metal wall.

A helical m=1 instability, with wavelength $2\pi/k$ is assumed to deform the plasma column into a solenoid, with the same wavelength, wound on a surface $r = r_o$, where r_o is the displacement amplitude. The toroidal plasma current flows along the helical coordinate (r_o, ζ_o) with $\zeta_o = \theta + kz = $ constant. The azimuthal component of the plasma current generates toroidal magnetic field inside the helix and field in opposite direction for $r_o < r < r_3$. The inductance for the toroidal current increases when the current channel changes from axial to helical. For a total toroidal current I the axial component is $I/\sqrt{1 + (kr_o)^2}$ and the azimuthal component for one wavelength is $Ikr_o/\sqrt{1 + (kr_o)^2}$. The toroidal flux generated by the azimuthal component of the current inside the solenoid amounts to $\mu_o I k^2 r_o^3 /2\sqrt{1 + (kr_o)^2}$. In the experiment the flux

increase inside r_1 between t = 5 μs and t = 6.5 μs is 1.2×10^{-2} Wb while the reduction in B_z outside r_1 is 6×10^{-2} T. The average value of I over this period is 90 kA. For typical values at the end of the growth phase, when r_o = 3.3 cm and k has decreased to 30 m^{-1} (kr_o = 1), the flux increase for the helical model (r < r_o) will be 1.2×10^{-3} Wb, and outside the helix B_z will fall by 4×10^{-2} T. Thus the solenoidal effect appears to be sufficient to explain the observations quantitatively.

The increase in inductance observed in the experiment between t = 5 and t = 6 μs, is ascribed to the increase in magnetic energy resulting from the deformation of a straight filament into a helix. When a cylindrical plasma column is unstable to an m = 1 helical kink instability the plasma moves outwards with a helical and a radial velocity component. The kinetic energy of the motion can be a large fraction of the energy in the azimuthal field in a grossly unstable plasma. (The velocity of the plasma column during the large amplitude phase is about 5×10^4 ms^{-1} whereas the Alfvén speed is on average 1-2 $\times 10^5$ ms^{-1}.) If the plasma displacement deviates locally from the average (helical) value and the displacement amplitude is comparable to the radius of the wall the local average of $B_z(r_2)$ can differ from the average of $B_z(r_2)$ over a large section of the torus. The sign of the difference between $B_z(r_2)$ and < $B_z(r_2)$ > depends on the relative amplitudes of the local radial displacement and the averaged displacement. For the effect to occur it is essential that the plasma displacement varies both in azimuthal and in longitudinal direction, the simplest case being a helical displacement. The sign of the difference signal is random when monitored over many discharges, as expected for a randomly varying displacement amplitude.

The cross-section of a thin helical plasma column inside a conducting shell will change in shape when the helical amplitude increases and the plasma is expected to form an expanding helical crescent on the surface r = r_o. The plasma will expand until it has covered the surface

$r = r_o$, after which reconnection of plasma and field is possible by dissipation. The plasma expansion in azimuthal direction leads to a fall in plasma inductance, which reaches a minimum when the current density is homogeneous on the surface $r = r_o$. Flux amplification is expected to continue during the azimuthal expansion of a helical column, and will cease when the plasma reaches an axisymmetric state, as observed in the dI/dt and dΦ/dt signals of figure 2. An analytical solution for m=1 helical flow in a conducting cylinder with axisymmetric initial conditions has been obtained by Zueva and Solovev.[27] From their solution the plasma is shown to flow towards the conducting wall but on approach the plasma departs in opposite azimuthal directions. The flow pattern does not rejoin but the plasma retains the shape of a crescent since no dissipation is introduced in the calculation and reconnection is therefore not possible. Dissipative effects are included in numerical simulations of the experiment with 3D-MHD codes by Sykes and Wesson,[28] which lead to crescent shaped magnetic surfaces (isobars) while the flux inside the plasma is increased. Field reversal is created when the total flux is conserved. The driving mechanism is identified as an m=1 instability which grows to large amplitude. Reconnection of the crescent shaped plasma is obtained in the simulation within a few Alfvén transit times, after which the plasma is approximately axisymmetric. Results will be published elsewhere[29].

Analytically it has been shown by e.g. Whiteman[30], Solovev and Shafranov[31] that a second magnetic axis emerges as a result of a large amplitude helical instability, while cylindrical isobars are deformed into helically twisted crescents. The first magnetic axis is located inside the helical column, while the second axis corresponds to the central axis of the helix. The second axis arises from the field generated by the helical current. In Kadomtsev's recent theory[32] the second magnetic axis, which arises as a consequence of a large amplitude internal m=1 helical kink

instability in a Tokamak, becomes more important than the initial axis and a restoration of axisymmetry is predicted in a dissipative plasma. The final effect of the instability is a radial expansion of the current distribution, a phenomenon also observed in the pinch experiment.

5. CONCLUSION

Amplification of the toroidal flux within the plasma has been observed in stablized z-pinches in HBTX-1 during an MHD instability, which leads to reversal of the field outside the plasma when the total toroidal flux is conserved.

The instability associated with the flux enhancement is an MHD helical kink instability with $m=1$, $k \sim 60 \ m^{-1}$, originating in the central region where most of the plasma current flows. The measured growth rate, wavelengh, and field perturbations are predicted with a linear MHD-stability code, including dissipative effects, using the measured field distributions. The predictions agree with observations until field perturbations become larger than 30% of the main field.

The increase in toroidal flux inside the plasma and hence the reversal of field in the outside region is associated with the non-linear stage of the instability, during which the plasma becomes redistributed. The observed level of flux increase is explained with a helical filament model of the large amplitude stage of the instability, using experimental values for the wavelength and radius of the helix.

The redistribution of the configuration leads to an approximately axisymmetric reversed field pinch for which the plasma radius is larger than before the instability. The effective radial expansion as a result of a large amplitude $m=1$ helical kink instability has been explained with analytical models by other authors while simulation of the development of the instability with a 3D-MHD code leads to good qualitative agreement with experimental observations.

The pinch ratio at the plasma boundary falls to 1.6 during the instability and then stays approximately constant which indicates that the plasma has reached a final state. This confirms a trend predicted with Taylor's theory.

REFERENCES

(1) Bickerton, R. J., Proc. Phys. Soc., $\underline{72}$ 466 (1958) 618.

(2.) Cowling, T. G., Mon. Not. R. Astro. Soc. $\underline{94}$ (1933) 39.

(3) Backus, G. E., Chandrasekhar, S., Proc. Nat. Acad. Sci. Wash. $\underline{42}$ (1956) 105.

(4) Robinson, D. C., Phys. Fluids, $\underline{11}$ 9 (1968) 2054.

(5) Lees, D. J., Rusbridge, M. G., Proc. 4th International Conf. Ionization
Phenomena in Gases, Uppsala, August 1959, $\underline{2}$ (1960) 954, N.H.P.C. Amsterdam.

(6) Butt, E. P., Carruthers, R., Mitchell, J. T., Pease, R. S., Thonemann, P. C.,
Bird, M. A., Blears, J., Hartill, E. R., Proc. 2nd UN International Conf.
on the Peaceful Uses of Atomic Energy, $\underline{32}$ (1958) 42.

(7) Burtsev, V. A., Glukhikh, V. A., Zawarin, D. E., Komar, E. G., Larionov,
B. A., Monoszon, N. A., Skotnikov, V. V., Stolov, A. M., Proc. Conf. on
Plasma Physics and Controlled Nuclear Fusion Research, Salzburg
CN 10/236 (1961).

(8) Colgate, S. A., Ferguson, J. P., Furth, H. P., Proc. 2nd UN International
Conference on the Peaceful Uses of Atomic Energy $\underline{32}$ (1958) 129.

(9) Conner, J. P., Hagerman, D. C., Honsaker, J. L., Karr, H. J., Mize, J. P.,
Osher, J. E., Phillips, J. A., Stovall, E. J., Proc. 2nd UN International
Conf. on the Peaceful Uses of Atomic Energy $\underline{32}$ (1958) 297.

(10) Allen, N. L., Balfour, D., Clock, V. C., Green, L. A., Hemmings, R. F.,
Hughes, T. P., Hunt, S. E., Jordan, B., Liley, B. S., Payne, R. M.,
Read, J. E., Ware, A. A., Williams, R. V., Young, K. M., Plasma Physics
(J.N.E. Part C) $\underline{4}$ (1962) 375.

(11) Kadomtsev, B. B., Proc. Conf. on Plasma Physics and Controlled Nuclear
Fusion Research, Salzburg (1961) CN 10/227. Nuclear Fusion Suppl. $\underline{3}$
(1962) 969.

(12) Sawyer, G. A., Scott, P. L., Stratton, T. E., Phys. Fluids $\underline{2}$ (1959) 47.

(13) Buffa, A., Costa, S., Nalesso, G. F., Malesani, G., 7th European Conf.
on Controlled Fusion and Plasma Physics, Lausanne, $\underline{I}$ (1975) 40.

(14) Butt, E.P., Newton A.A., Verhage, A.J.L., 3rd Topical Conf. on Pulsed High Beta Plasmas, Culham (1975) Paper C2.1.

(15) Butt, E.P., Gowers, C.W., Gribble, R.F., Li Yin-An, Newton, A A., Robinson. D.C., Verhage, A.J.L., Bodin, H.A.B., Taylor, J.C., Sharp, W.J., Proc. 5th Conf. on Plasma Physics and Controlled Nuclear Fusion Research, Tokyo 1974.

(16) Robinson, D.C., Verhage, A.J.L., 2nd International Congress on Waves and Instabilities in Plasmas, Innsbruck (1975), Book of Abtracts, P 9.

(17) Butt, E.P., Gowers, C.W., Mohri, A., Newton, A.A., Robinson, D.C., Verhage, A.J.L., Watts, M.R.C., Li Yin-An, Bodin, H.A.B., 7th European Conf. on Controlled Fusion and Plasma Physics, Lausanne, $\underline{I}$ (1975) 30.

(18) Verhage, A.J.L., Robinson, D.C., 3rd Topical Conf. on Pulsed High Beta Plasmas, Culham (1975) Paper B1.5.

(19) Taylor, J.B., Phys.Rev.Lett. $\underline{33}$ (1974) 1139.

(20) King, R.E., Robinson, D.C., Verhage, A.J.L., Phys.D:Appl.Phys. $\underline{5}$ (1972) 2015.

(21) Bobeldijk, C., Oomens, A.A.M., Van der Laan, P.C.T. Nuclear Fusion (1973) 121.

(22) Van Heyningen, R.J.J., Maris, D.J., Bobeldijk, C., Van der Laan, P.C.T., Plasma Phys. $\underline{14}$ (1972) 205.

(23) Crow, J.E., Robinson, D.C., 2nd Topical Conf. on Pulsed High Beta Systems, Garching (1972) Paper C1.

(24) Crow, J.E., Killeen, J., Robinson, D.C., 6th European Conf. on Controlled Fusion and Plasma Physics, Moscow (1973) 269.

(25) Dibiase, J.A., "Numerical Studies of Resistive Instabilities in Diffuse Pinches", Ph.D Thesis, May 1974, LLL Report UCRL-51591.

(26) Dibiase, J.A., Killeen, J., Robinson, D.C., Schnack, D., 3rd Topical Conf. on Pulsed High Beta Plasmas, Culham (1975) Paper B1.9.

(27) Zueva, N.M., Solov'ev, L.S., Preprint No 95 of the Institute of Appl. Maths, USSR Academy of Sciences, Moscow, 1975, also: Zueva, N.M., Solov'ev, L.S., Morozov, A.I. Letters to Zh.Eksp.Teor.Fiz. $\underline{23}$, 5 (1976) 284.

(28) Sykes, A., Wesson, J.A., 7th European Conf. on Controlled Fusion and Plasma Physics, Lausanne, $\underline{I}$ (1975) 11.

(29) To be published in the Proceedings of the 6th IAEA Conference on Plasma Physics and Controlled Nuclear Fusion, Berchtesgaden, Germany, 1976.

(30) Whiteman, K.J., Culham Laboratory Preprint, CLM-P 14 (1962).

(31) Solov'ev, L.S., Shafranov, V.D., in Reviews of Plasma Physics, Vol. $\underline{5}$, pp 90-91, Atomizdat Moscow (1967) and Consultants Bureau, New York (1970).

(32) Kadomtsev, B.B., Fizika Plasmy, $\underline{1}$, 5 (1975) 710.
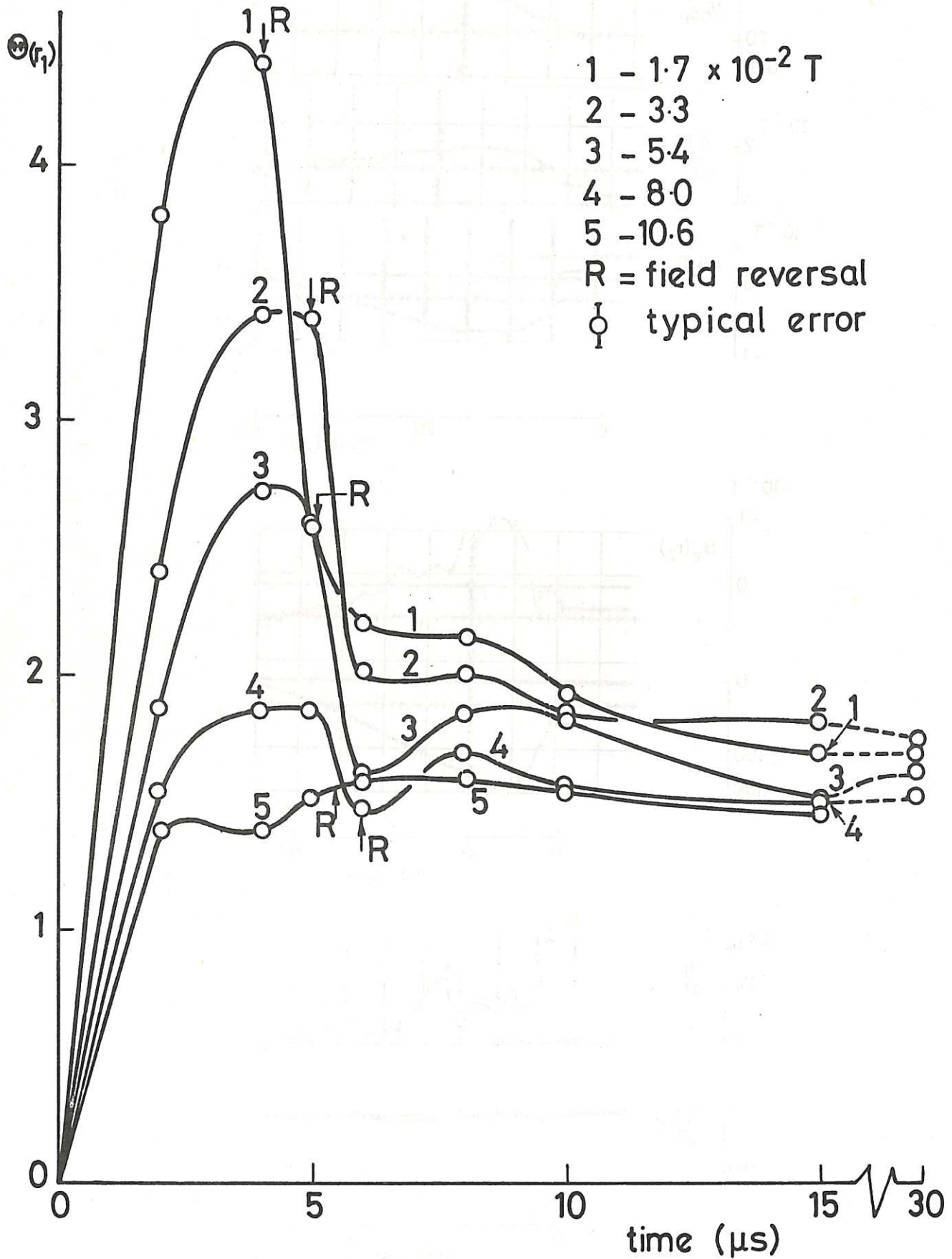
Fig. 1 The pinch ratio, taken at the plasma boundary, as a function of time for 5 different values of the trapped flux. The plasma current reaches a maximum of about 150 kA at t = 15 μs. The change in sign of $B_z(r_2)$ is marked with R.
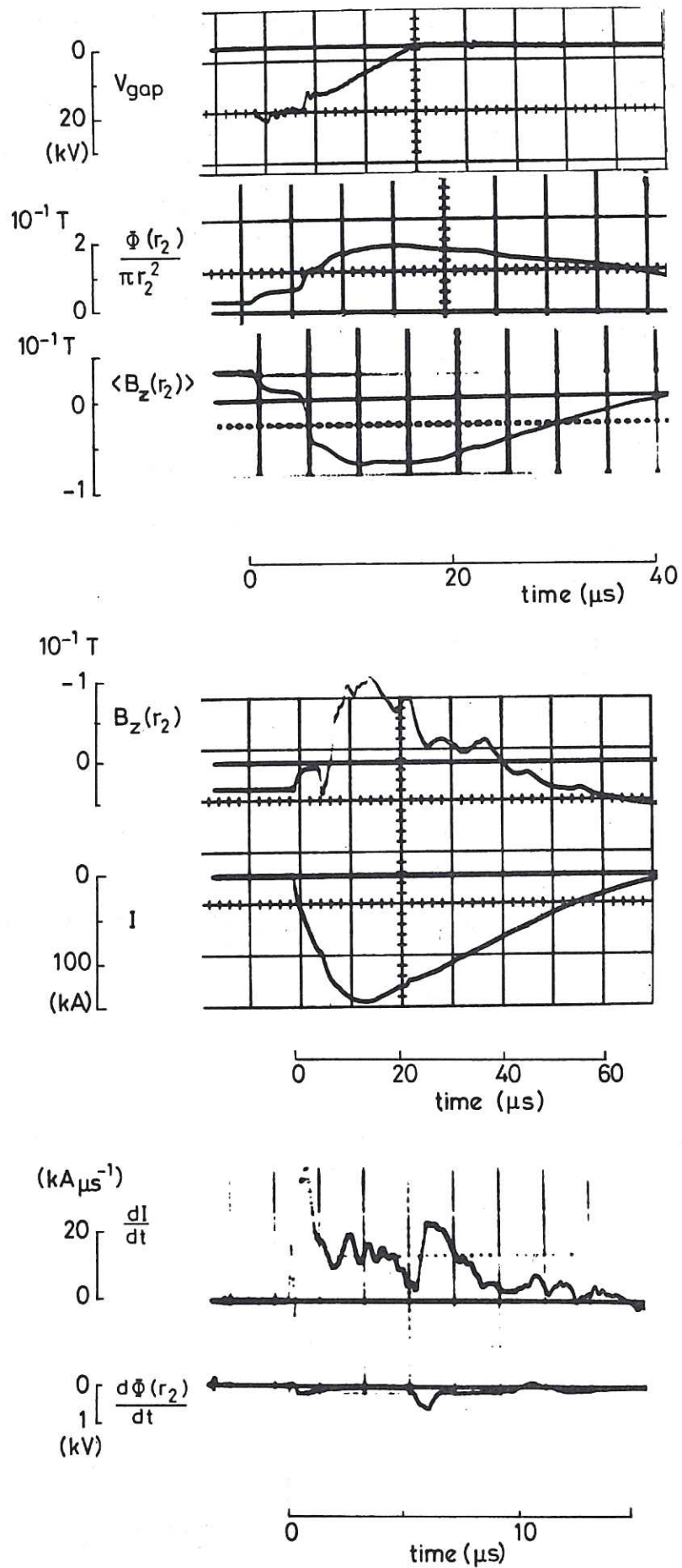
Fig. 2 Main parameters of the stabilized z-pinch, with field reversal. The upper oscillograms show
the voltage across a feeder gap in the shell, the toroidal flux inside the conducting shell, and B_z outside
the plasma averaged over a quarter of the torus. In the middle are B_z outside the plasma averaged over
a thin annulus, and the plasma current, on a different timescale. The lower two oscillograms show the
unintegrated signals of plasma current and toroidal flux on a shorter timescale.
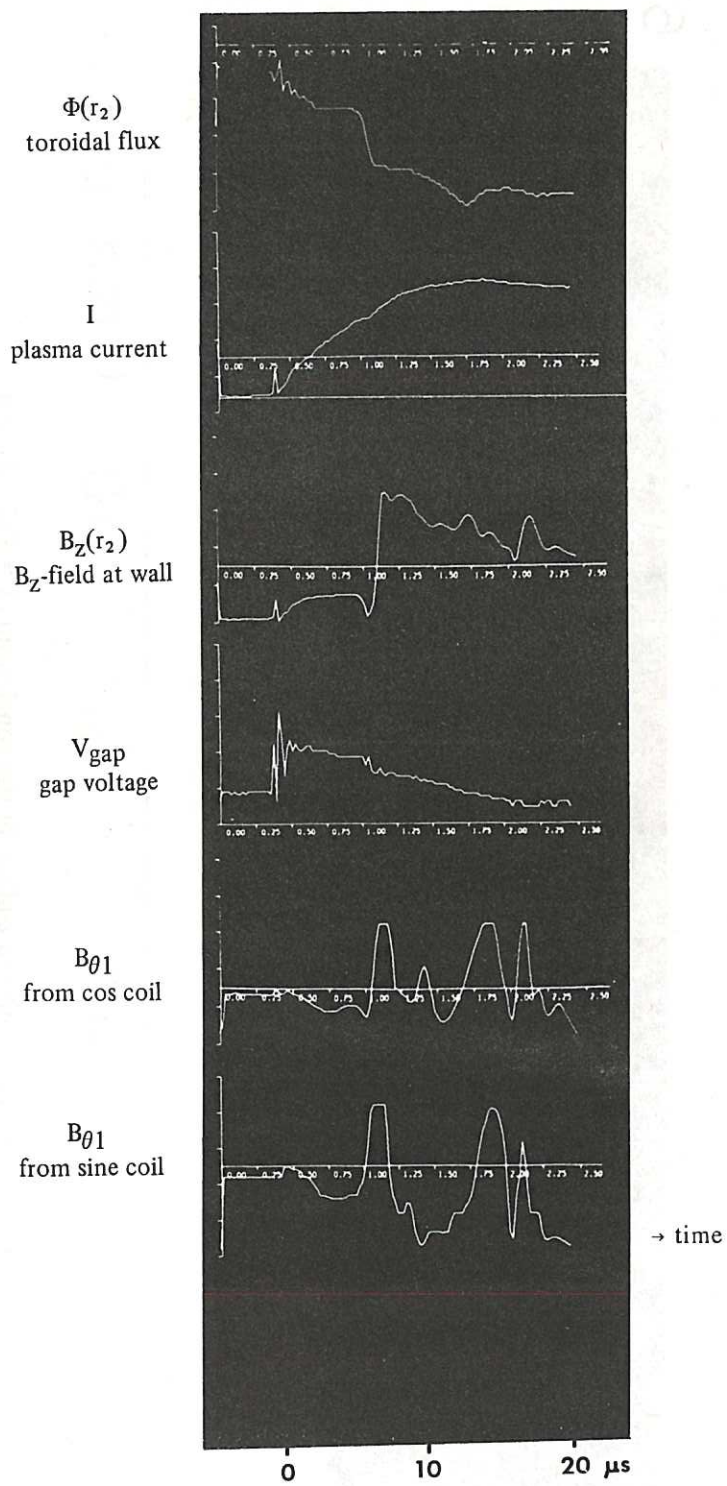
Fig. 3   Main parameters and amplitudes of the m=1 component of B_θ as recorded with synchronized analog-digital converters for the same discharge of which data are shown in figure 2.
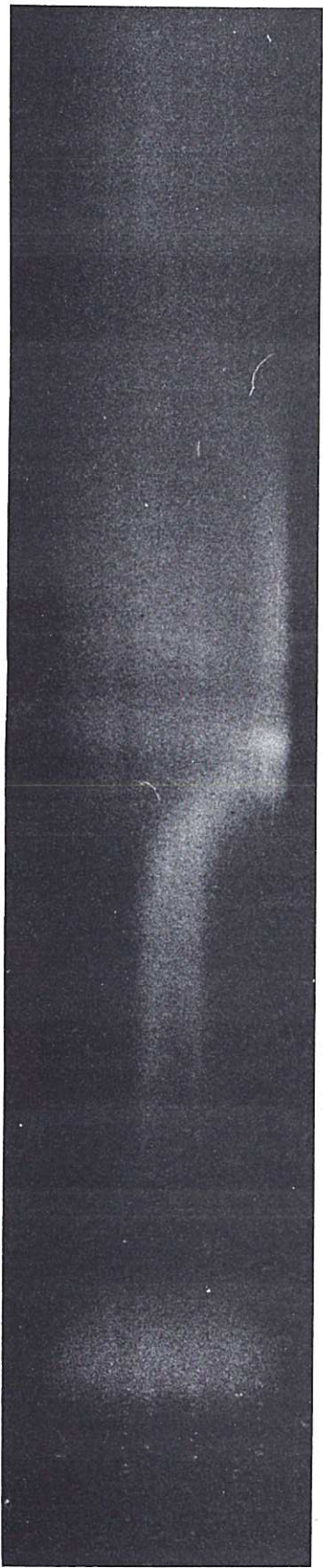
Fig. 4 Streak photograph of the stabilized z-pinch in the continuum ($\lambda = 535 \pm 15$ nm). The time at which $B_z(r_2)$ reverses is marked R.
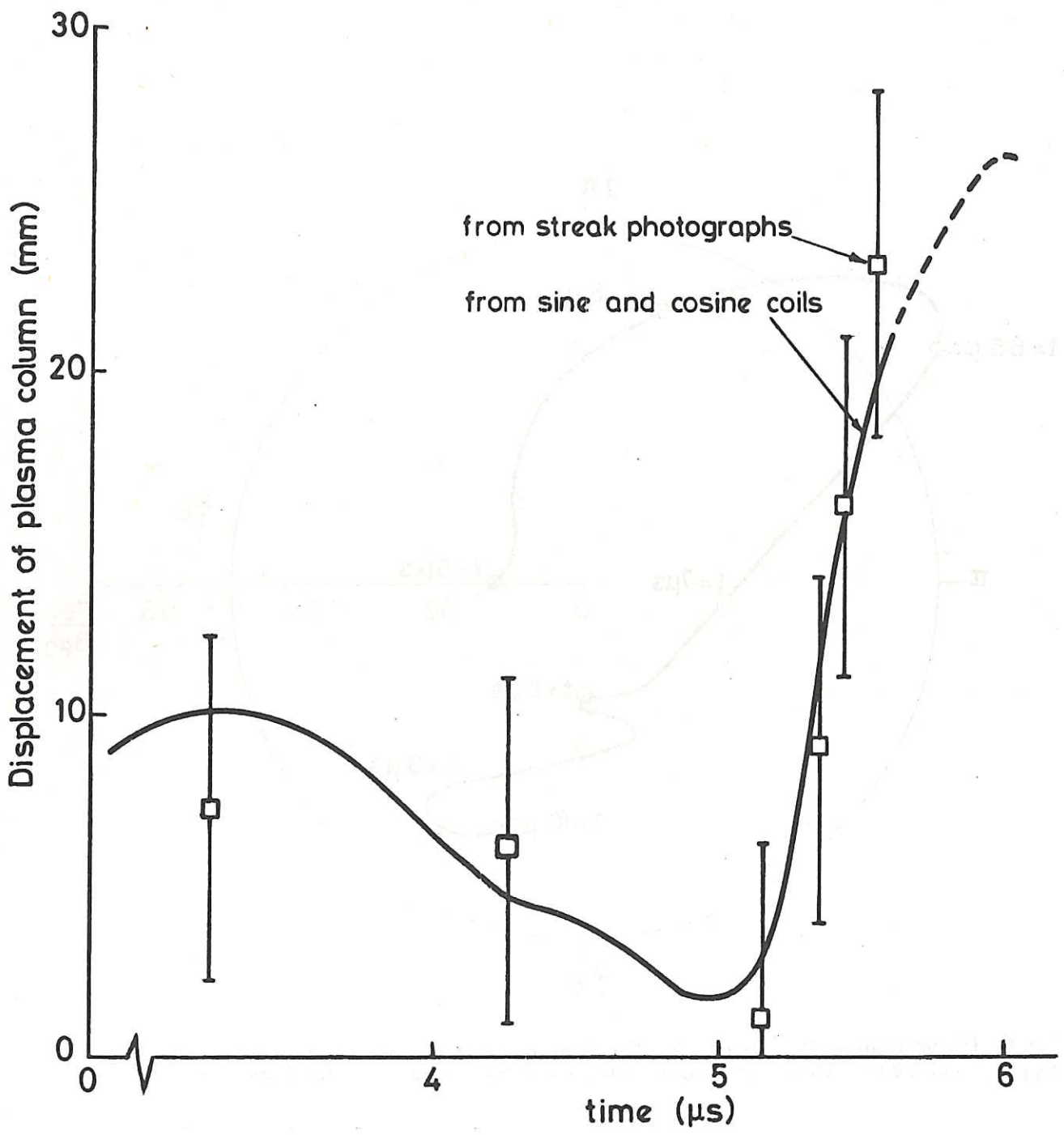
Fig. 5   Displacement of the plasma column as a function of time derived from streak photographs and from sine and cosine coils, assuming that the plasma column is straight.
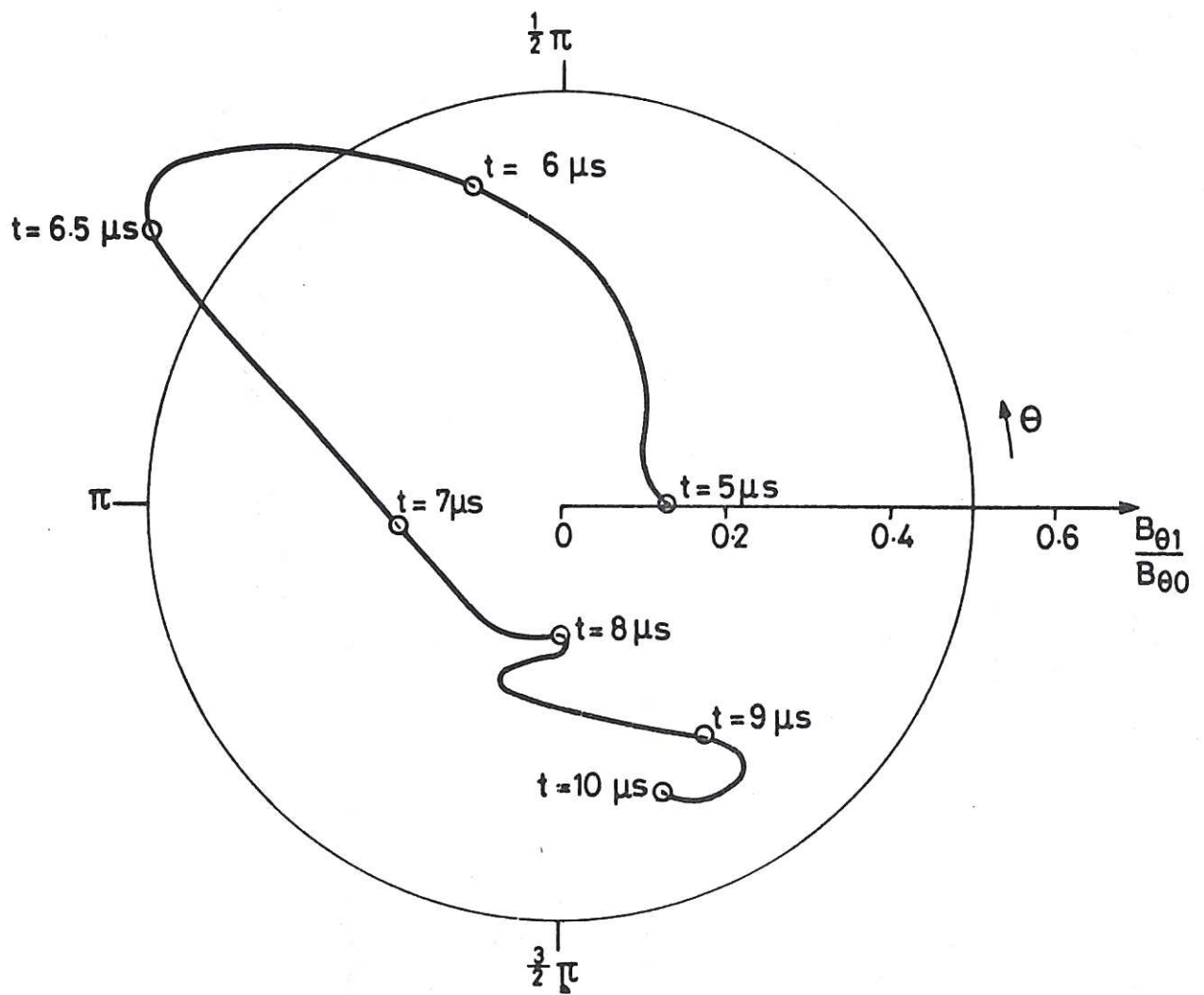
Fig. 6 The position of the centre of the plasma in the azimuthal plane represented by the ratio $B_{\theta 1}/B_{\theta 0}$ and the azimuthal angle θ during the growth and saturation of the instability.
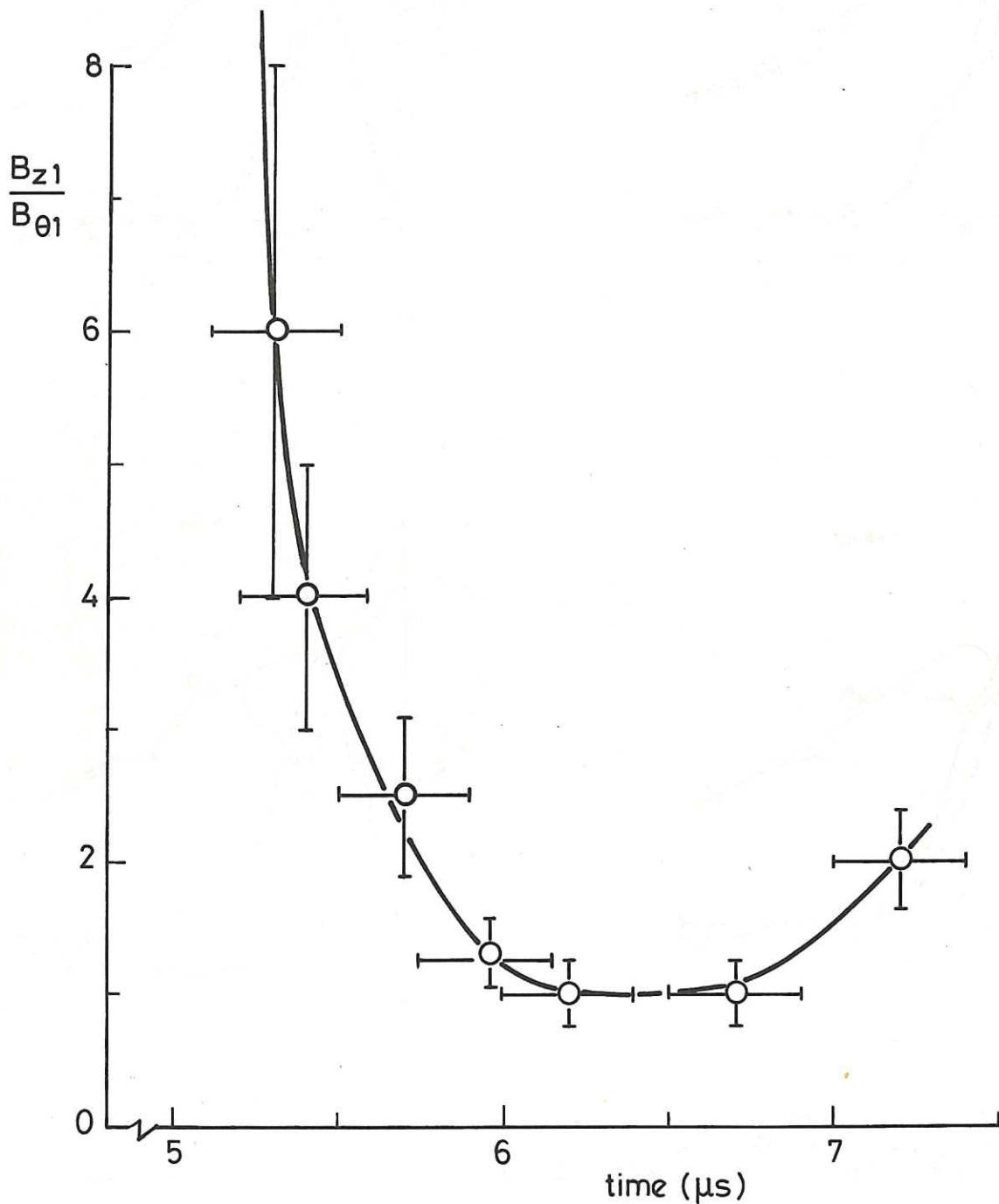
Fig. 7 The ratio of the first harmonics of B_z and B_θ measured near the conducting wall $r = r_2$ as a function of time during growth and large amplitude stage of the m=1 helical kink instability. The wavenumber k of the instability is equal to $B_{z1}/r_2B_{\theta1}$. (The displacement, for a straight column, at the position of the circle is 19 mm).
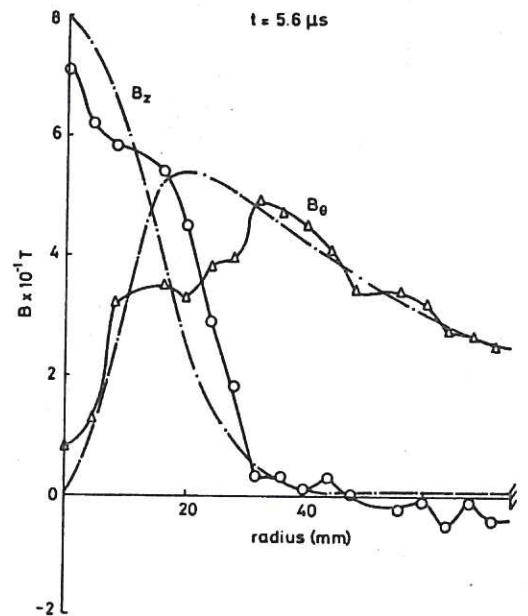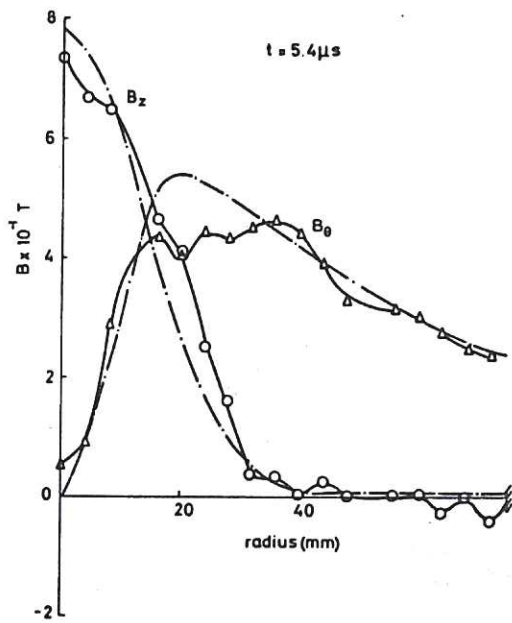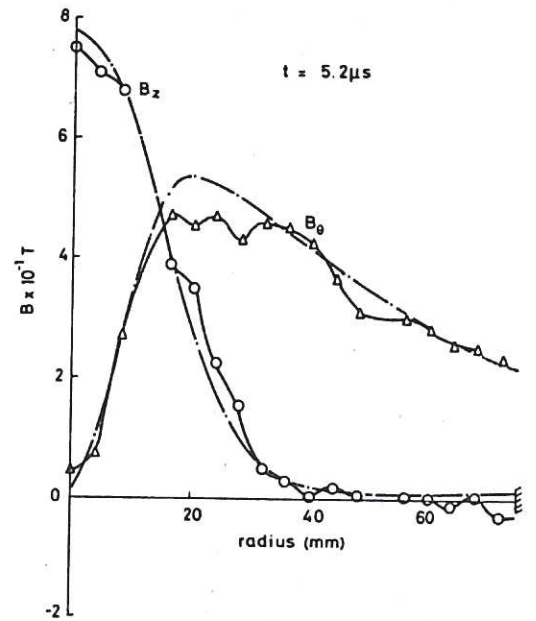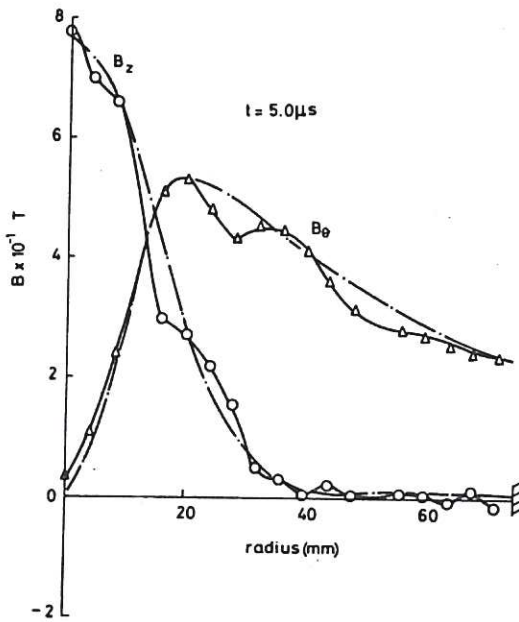
Fig. 8 Comparison of the extrapolated unperturbed magnetic field and the measured field profiles (experimental points on solid line) at four different times during the growth of the instability. The differences between the two sets of profiles is interpreted as perturbations due to the instability.
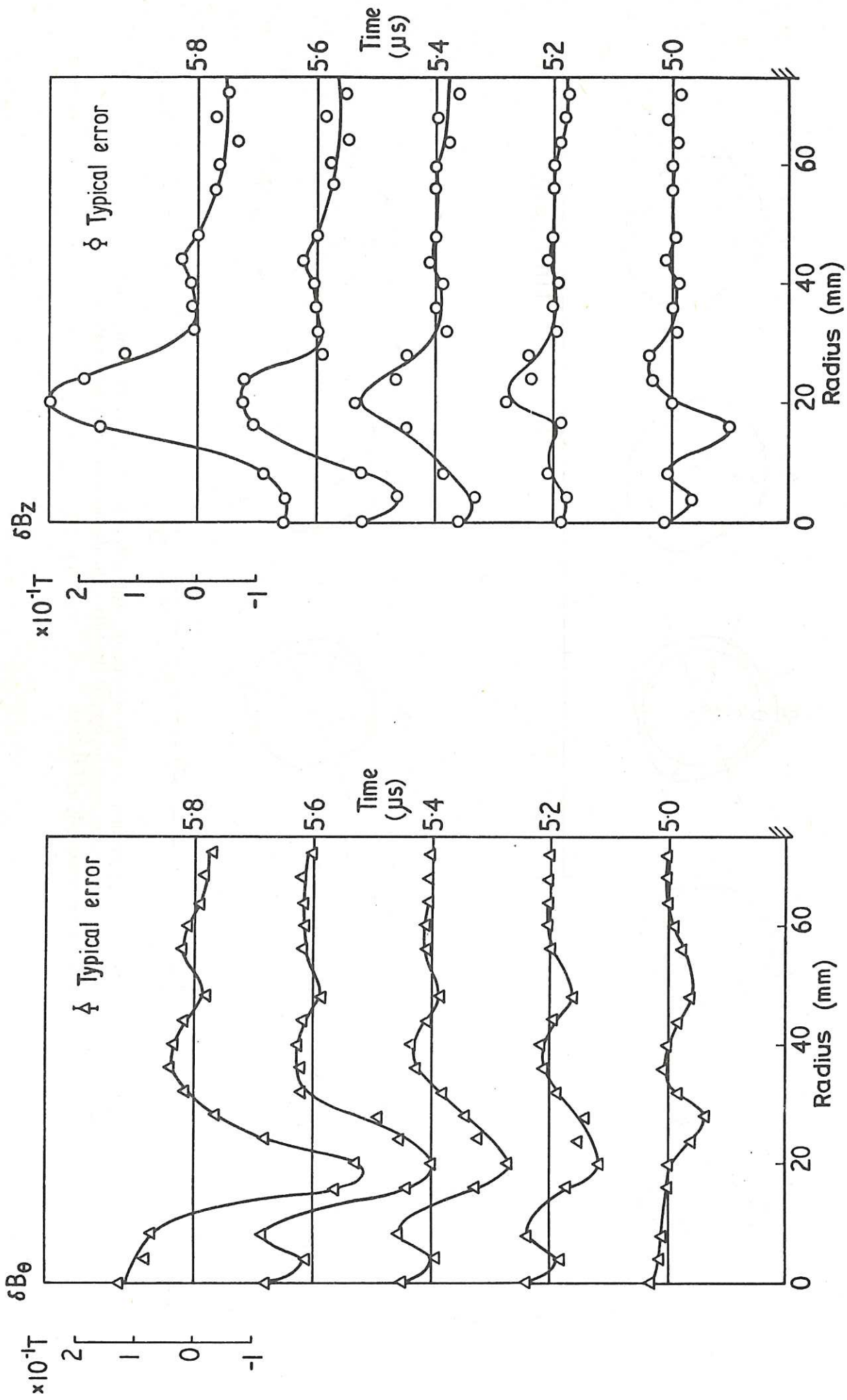
Fig. 9 Radial dependence of the measured perturbations in B_θ and B_z during the growth of the m=1 helical kink instability. The field perturbations are obtained as the difference between measured and extrapolated field of figure 8.
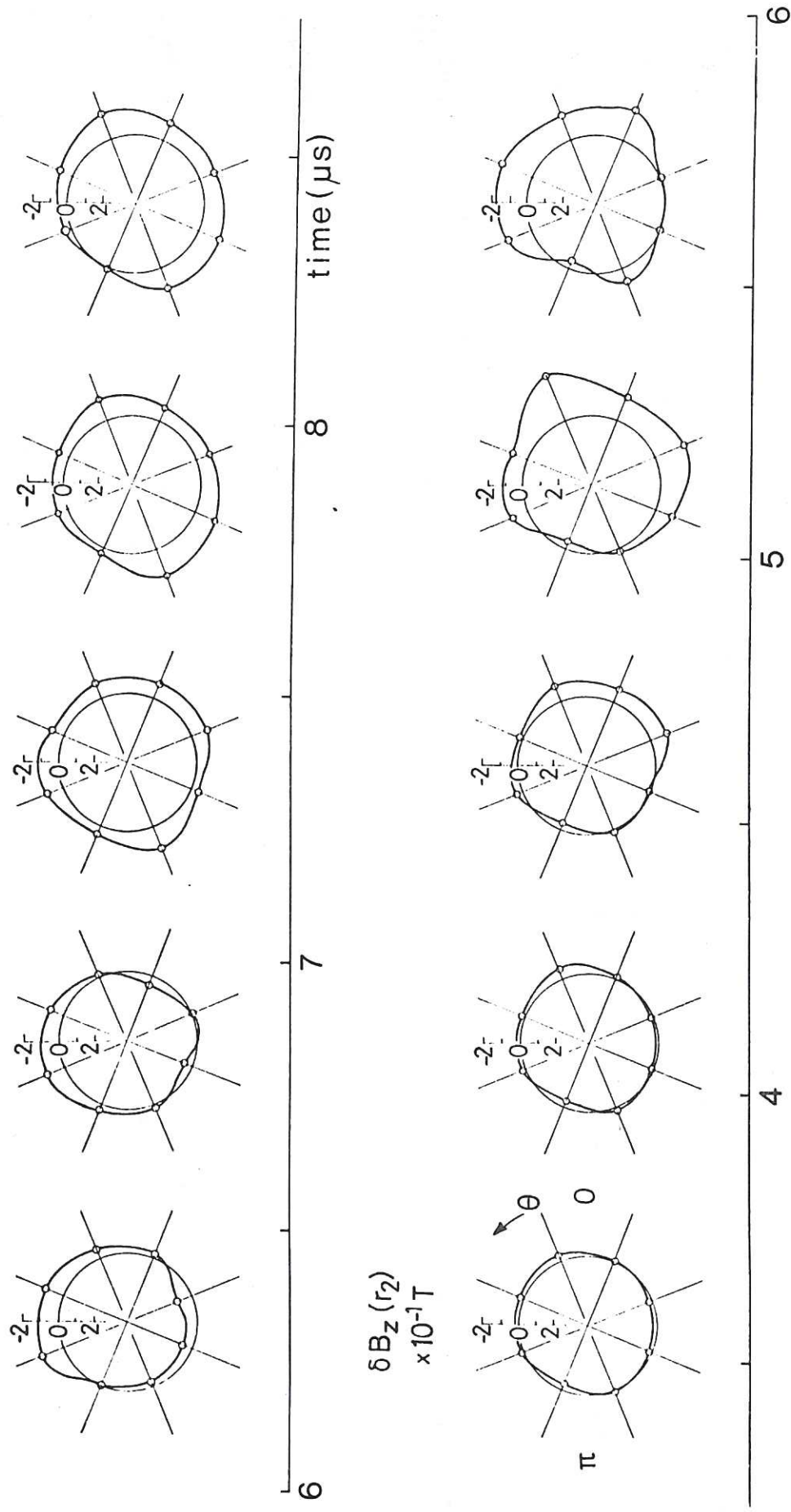
Fig. 10 Perturbations of B_z measured near the conducting wall at 8 positions in minor azimuth for different times. The circle depicts the cross-section of the tube. The distance between the contour and the circle represents the amplitude of $\delta B_z(r_2)$.

$$\Phi (r_1,t) = \int\limits_0^{r_1} B_z \, 2\pi r \, dr$$

$$\chi (r_1,t) = \lambda \int\limits_0^{r_1} B_\theta \, dr \qquad \lambda = 10 \, cm$$

from magnetic probes
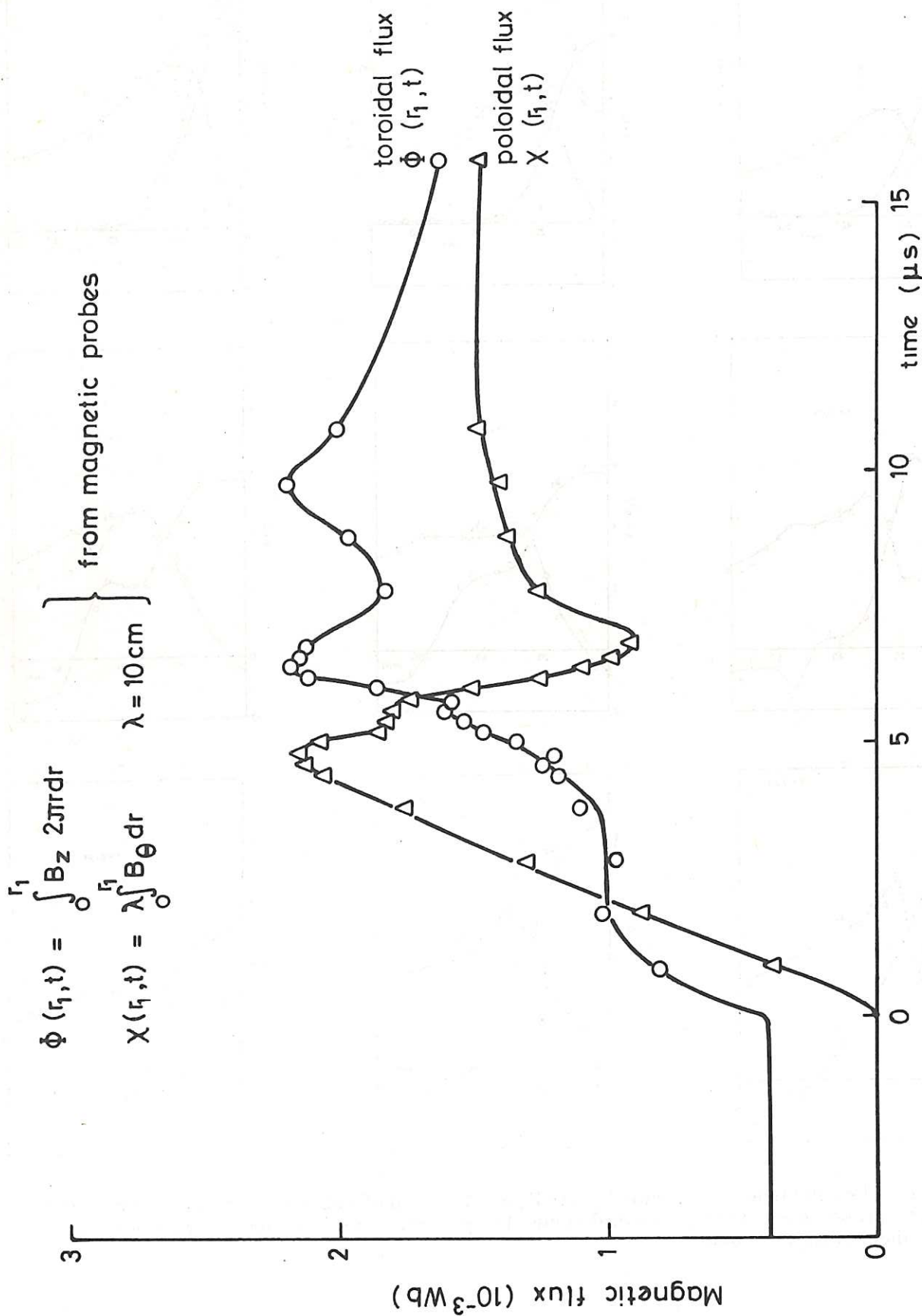
Fig. 11   Toroidal and poloidal flux as a function of time for a stabilized z-pinch with the plasma current crowbarred at t = 5 μs. The helical flux is conserved between t = 5 μs and t = 7 μs when the average wavelength λ is 10 cm.
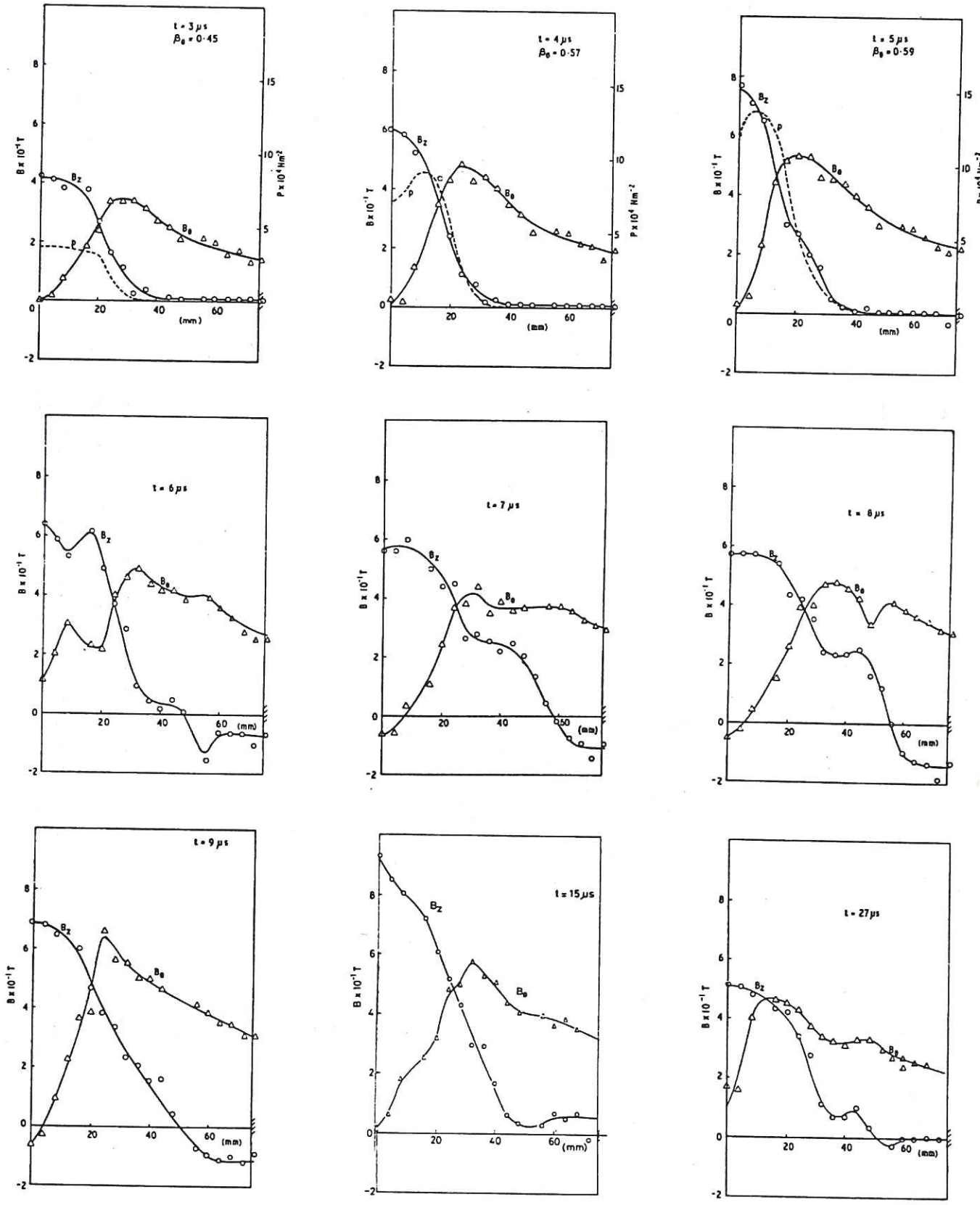
Fig. 12 Magnetic field components B_θ and B_z as a function of radius and time as measured with magnetic probes inserted along a vertical radius. The pressure profiles are derived from the fields before the plasma is unstable.
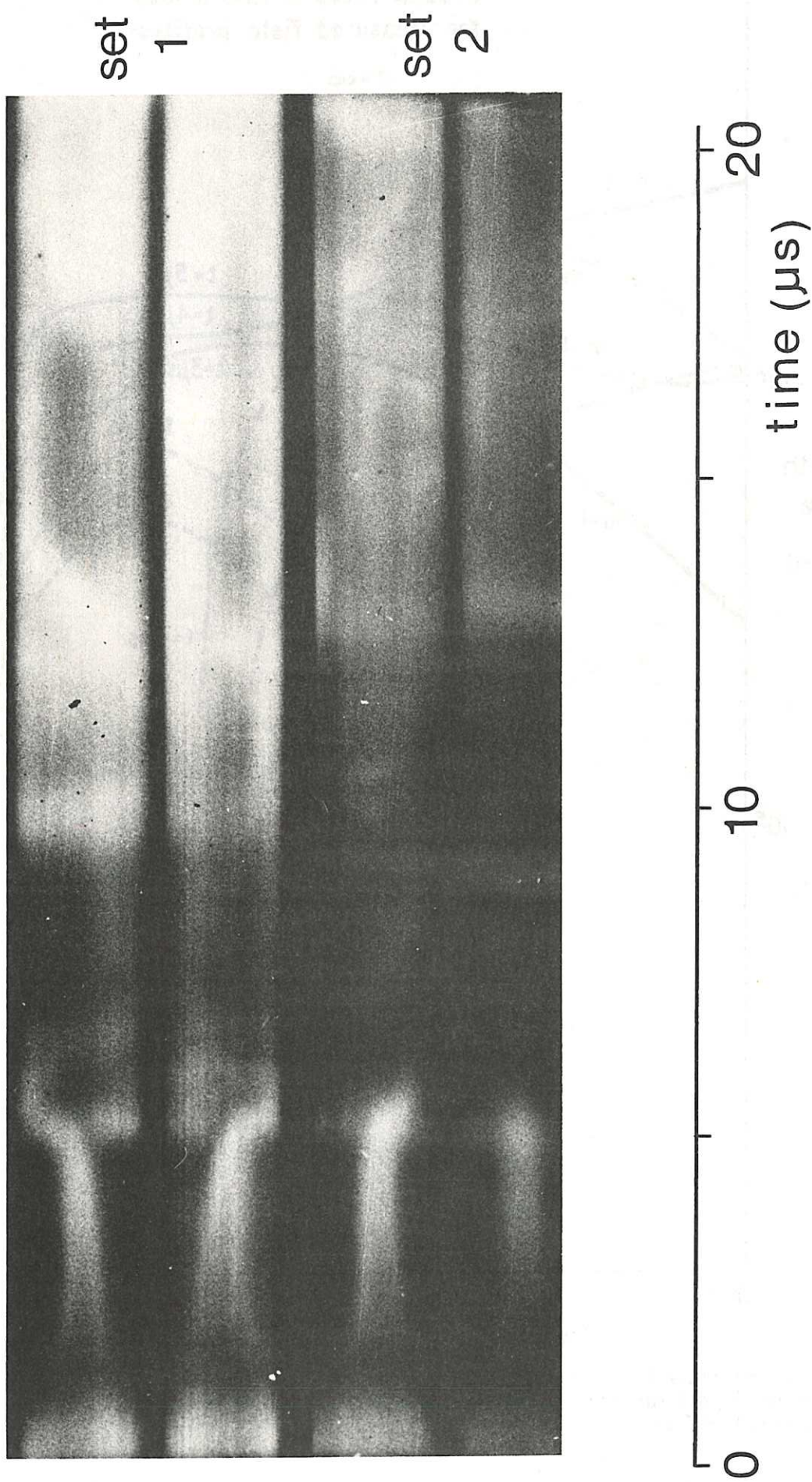
Fig. 13   Streak photographs of the plasma taken in two cross-sectional planes 26 cm apart and at two orthogonal positions in each plane. Only the radiation in the continuum $\lambda = 535 \pm 15$ nm was used. Each of the streak photographs covers the diameter of the tube with a radius of 6 cm, the same as in figure 4.
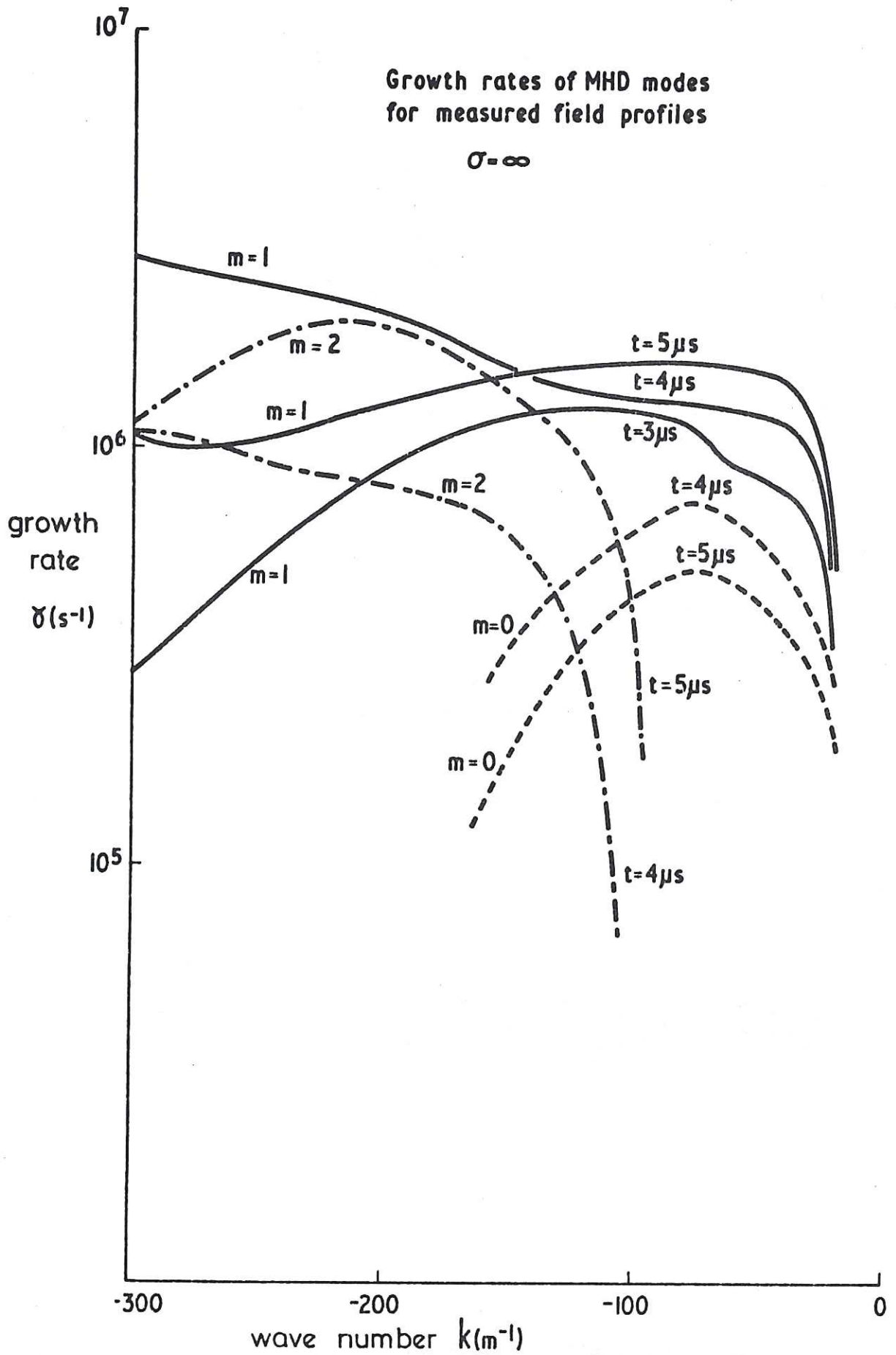
Fig. 14 Growth rates of ideal MHD-modes with m=0,1,2 as a function of wavenumber, computed for the radial pitch function derived directly from the measured field profiles of figure 12 at t = 3 μs, t = 4 μs, and t = 5 μs.

Growth rates of MHD-modes
for matched field profiles

$\beta_\Theta = 0.58$. $t = 4$ μs

——— $\sigma = \infty$ MHD

– – – σ finite

· · · · · · · σ, χ, ν finite

growth
rate
γ (s^{-1})

10^6

10^5

m = 1

m = 0

-300   -200   -100   0   100
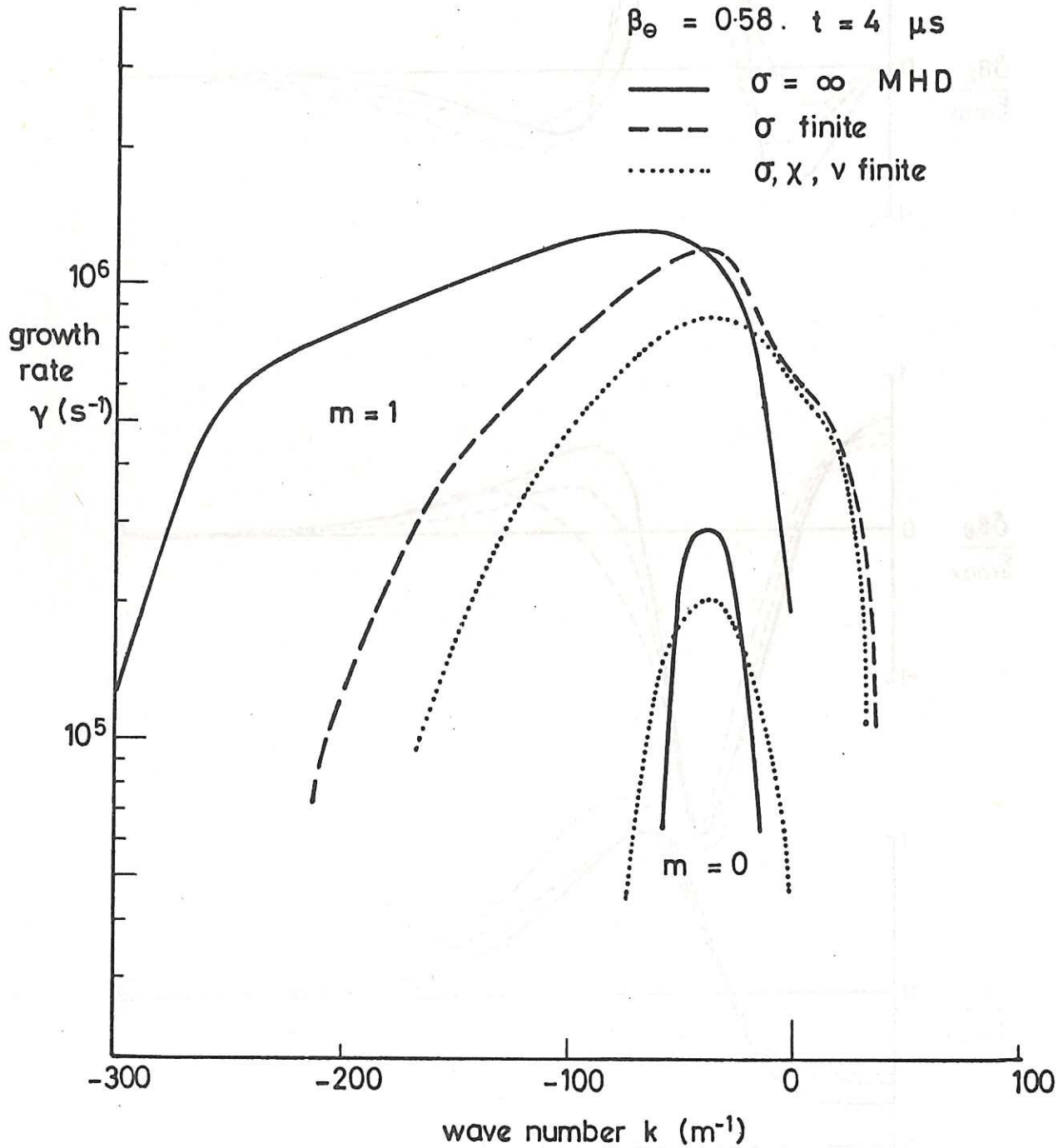
wave number k (m^{-1})

Fig. 15   The influence of dissipative effects on the growth rates of m=0 and m=1 as a function of
wavenumber, computed for an analytic pitch function matching the field profiles. The growth rate
for m=2 is negligibly small.
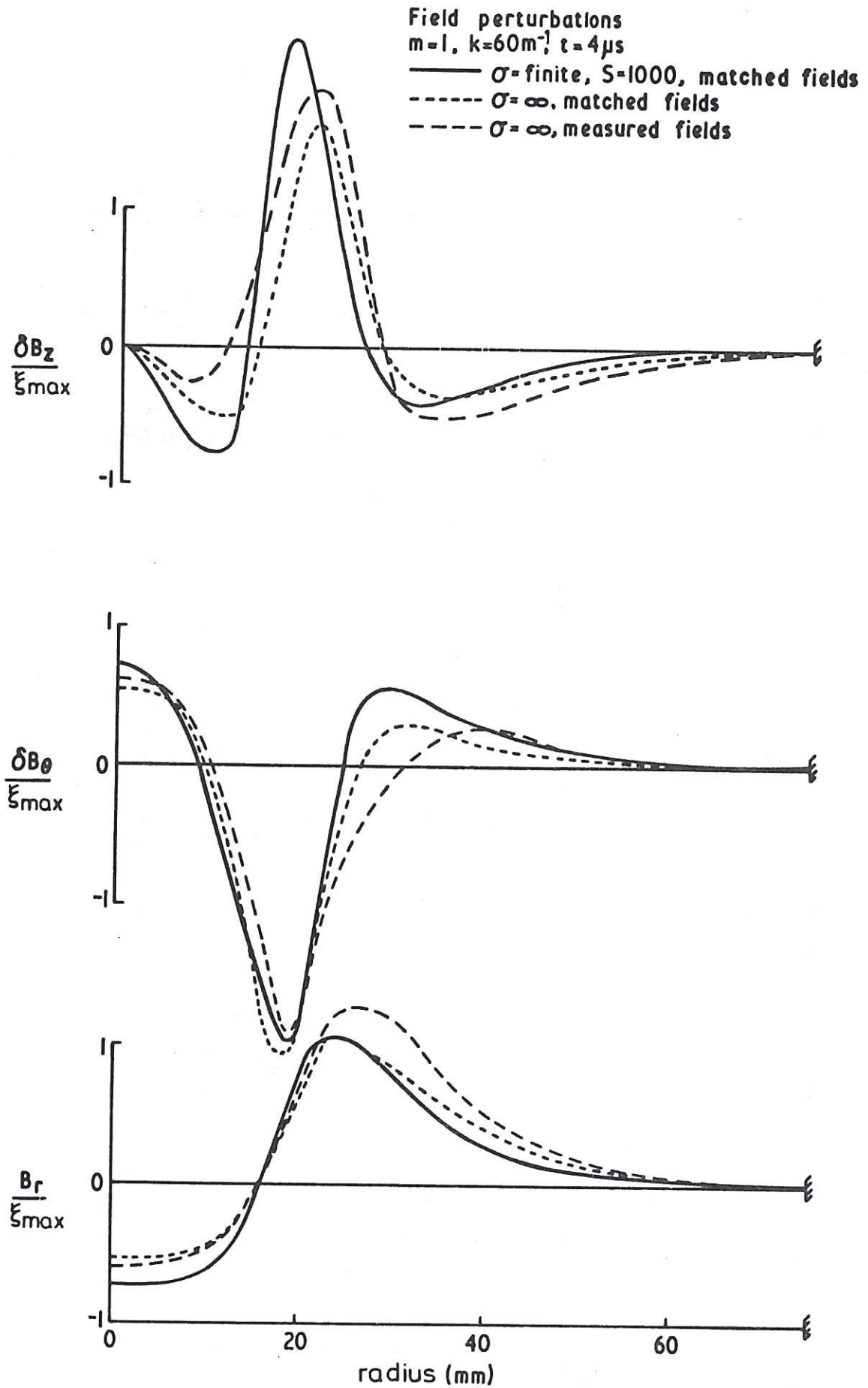
Fig. 16   The radial distributions of the normalized field perturbations for m=1, k = 60 m^{-1} as predicted with ideal MHD and resistive MHD computations. The influence of pitch matching on the perturbations is also shown.
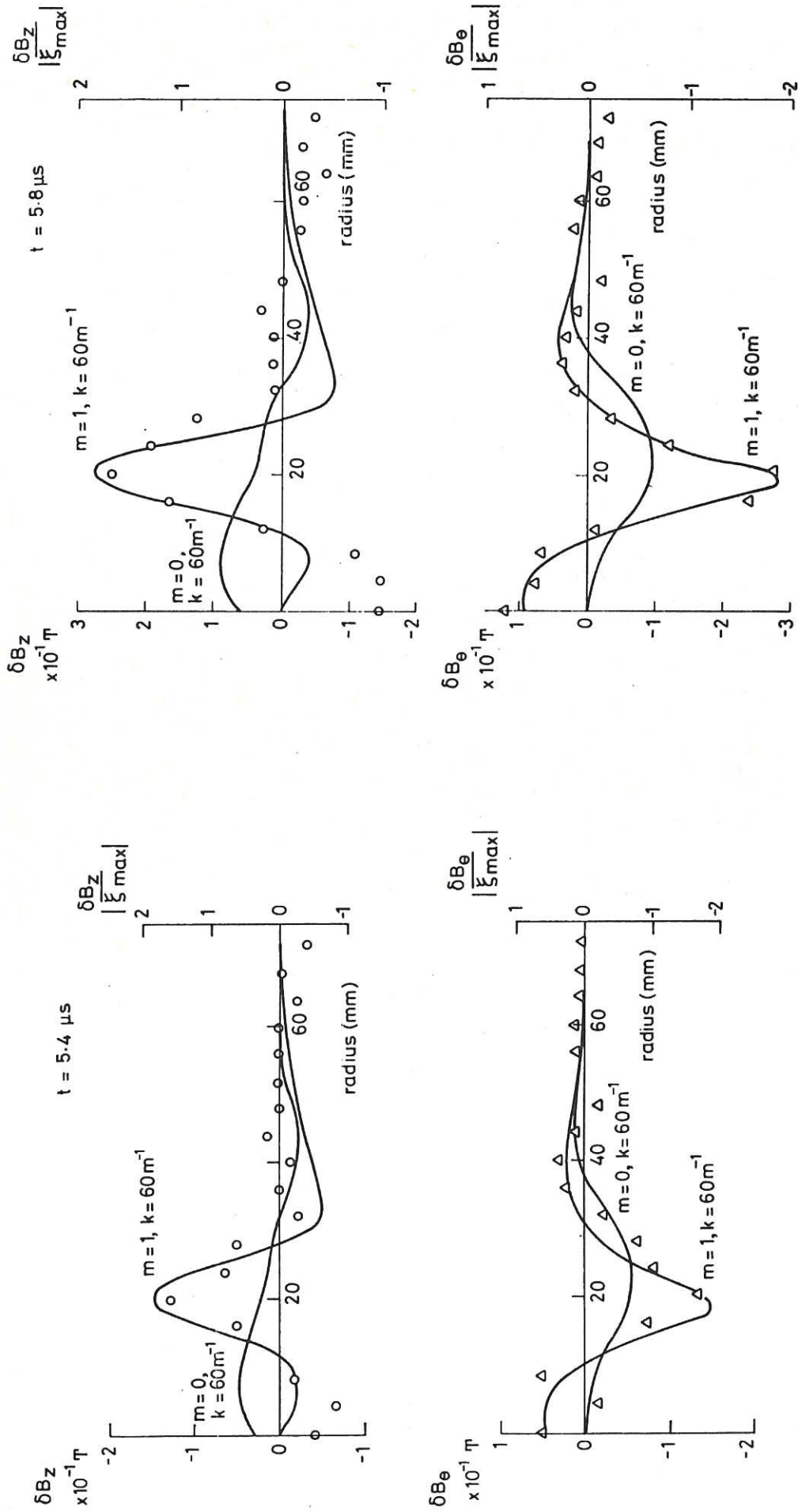
Fig. 17 Comparison of the measured field perturbations (experimental points) from figure 9 at t = 5.4 μs and t = 5.8 μs with the computed normalized perturbations, for m=0 and m=1 (solid lines) derived from the measured field profiles at t = 4 μs in the limit of ideal MHD.